Published in final edited form as:
J Magn Reson Imaging. 2010 January ; 31(1): 142–148. doi:10.1002/jmri.22001.

Imaging cerebral microbleeds using susceptibility weighted imaging: one step toward detecting vascular dementia

Muhammad Ayaz, PhD[1,2], **Alexander S. Boikov, BA**[1,5], **E. Mark Haacke, PhD**[1,2,3], **Wolff M. Kirsch, MD**[4], and **Daniel K. Kido, MD**[3]

[1]The MRI Institute for Biomedical Research, Detroit, Michigan

[2]Department of Neurology, Massachusetts General Hospital, Boston, Massachusetts

[3]Department of Radiology, Loma Linda University, Loma Linda, California

[4]Department of Neurosurgery, Loma Linda University, Loma Linda, California

[5]Wayne State University School of Medicine, Detroit, Michigan

Abstract

Purpose—To monitor changes in the number of cerebral microbleeds (CMBs) in a longitudinal study of healthy controls (HC) and mild-cognitively impaired (MCI) patients using susceptibility weighted imaging (SWI).

Materials and Methods—SWI was used to image 28 HC and 75 MCI patients annually at 1.5T over a four-year time period. Magnitude and phase data were used to visualize CMBs for the first and last scans of 103 subjects.

Results—Preliminary analysis revealed that none of the 28 HC had more than three CMBs. In the 75 MCI patients, five subjects had more than three CMBs in both first and last scans, while one subject had more than three bleeds only in the last scan. In five of these six MCI patients, the number of CMBs increased over time and all six went on to develop progressive cognitive impairment (PCI). Out of the 130 total CMBs seen in the last scans of the six MCI cases, most were less than 4 mm in diameter.

Conclusion—SWI can reveal small CMBs on the order of 1 mm in diameter and this technique can be used to follow their development longitudinally. Monitoring CMBs may be a means by which to evaluate patients for the presence of microvascular disease that leads to PCI.

Keywords

susceptibility weighted imaging; cerebral microbleeds; vascular dementia

INTRODUCTION

The role of cerebral microbleeds (CMBs) in vascular dementia and aging is gaining more and more attention (1–7). Most of these studies include a large number of subjects and often discuss the role of cerebral amyloid angiopathy (8) as one of the main causes of intracranial hemorrhage (9–11). In magnetic resonance imaging (MRI), a CMB tends to manifest as a spherical hypointensity on conventional GRE T_2* images and has usually been taken to be

Corresponding Author: E. Mark Haacke, PhD, Wayne State University, MR Research Facility, Department of Radiology, HUH—MR Research G030/Radiology, 3990 John R Road, Detroit, MI 48201, Tel.: (313) 745-1395, Fax: (313) 745-9182, nmrimaging@aol.com.

5–10 mm in diameter (10,12). The broad and inconsistent range of sizes among studies has made efforts to detect them fraught with difficulty (10). Generally, CMB-related studies have been cross-sectional snapshots using GRE T_2* sequences to study patients with a variety of ages and conditions rather than longitudinal investigation of a series of subjects. The present work is novel in two ways: first, it is an analysis of data collected from the same subjects over the course of four years and second, instead of using conventional GRE T_2* to detect CMBs, we employ susceptibility weighted imaging (SWI) as described by Haacke, et al. (13). SWI is a high-resolution 3D GRE-T_2* sequence uniquely attuned to the detection of hemorrhage—opening the door to visualizing bleeds that have heretofore gone unnoticed. In fact, SWI has recently been shown to detect 67% more CMBs than a conventional GRE T_2* sequence (14). The purpose of the present work is to use SWI to track the progression of CMBs over time in a 4-year study of 75 mild-cognitively impaired (MCI) patients and 28 healthy controls. We hypothesize that an increase in CMBs will correspond to clinically determined cognitive decline.

MATERIALS AND METHODS

A series of 103 subjects—28 healthy controls and 75 patients with mild cognitive impairment—were evaluated in a longitudinal study of dementia (informed consent was obtained in all cases) (Figure 1). Medication, medical and smoking histories, thyroid function, serum B12 levels, and ApoE genotypes were determined. Subjects with diabetes, known cerebrovascular disease, head trauma, uncontrolled hypertension, iron metabolism abnormalities, and history of smoking were excluded.

All subjects were between ages 55 and 83 (average age = 73). Normal subjects were without objective or subjective memory deficits and within normal limits on neuropsychological testing (Global Clinical Dementia Rating (CDR) of 0, CDR memory component of 0 and a sum of CDR boxes of 1 or less at baseline). All MCI cases fulfilled the Mayo Clinic criteria for classification as having MCI multiple-domain impairment. More specifically, these criteria are: 1) a memory complaint confirmed by corrected Logical Memory testing or reports of the informant and a CDR of 0.5; 2) normal activities of daily living; 3) normal general cognitive function; 4) abnormal memory for age as measured by standard scores and education; and 5) a global CDR of 0.5 and no dementia (15).

All subjects were scanned on as close to an annual basis as possible, with some subjects being scanned more than once a year depending on their CDR. A primary analysis of the first and last scans of the 103 cases was distributed among two sites: three observers at one site reviewed 41 cases and four observers at another site reviewed the remaining 62. All CMB counts were reviewed by one experienced neuroradiologist with more than 5 years experience interpreting SWI data.

Imaging Parameters

A standard neuroimaging protocol was run, including diffusion weighted imaging (DWI), fast low-angle inversion recovery (FLAIR), magnetization-prepared gradient echo imaging (MPRAGE), and T_2 weighted imaging along with MR spectroscopy and SWI. The SWI acquisition parameters were: in-plane resolution = 0.5 mm × 1.0 mm; slice thickness = 2 mm; FOV = 256 mm × 256 mm; N_x = 512; N_y = 256; N_z = 48; TE = 40 ms; TR = 57 ms; FA = 20°; bandwidth (BW) = 78 Hz/pixel; and an interpolated in-plane voxel size = 0.5 mm^3. The phase images were high-pass (HP) filtered to remove background field effects and contrast-enhanced SWI magnitude images were created using a phase mask from the HP filtered phase images (13). Minimum intensity projections (mIPs) were performed over 5 slices of the SWI processed data, centered on the slice of interest. Focusing on the central 42 slices of the data, all of the original magnitude images, HP-filtered phase images and SWI

mIPs were used in the review process (Figure 2). When investigating changes in CMBs over time, images from all time points were put side by side and local geometry was used to match the regions of interest (ROIs).

White matter hyperintensities (WMH) were scored in all FLAIR images according to the Wahlund and Breteler scales for periventricular hyperintensity (16,17). Participants were classified as having <2 or 2+.

Detecting and Scoring CMBs with SWI

Sometimes referred to as "black dots," microbleeds appear as isolated, circular regions of signal hypointensity, usually taken to be between 5 and 10 mm in diameter on GRE T_2* images (10). Upon detecting a suspected CMB on magnitude, HP-filtered phase or SWI mIPs, all three types of images were reviewed. Observers reviewed several slices above and below the slice of interest in order to ensure that a suspected CMB was not simply a vessel cross-section. The mIPs over five slices served to further distinguish an isolated hypointensity from a vein. Once a potential CMB was identified, the HP-filtered phase image was zoomed by a factor of 4 to allow for a better tracing of its boundary using our in-house software SPIN (signal processing in NMR). Each CMB's boundary was selected to measure its volume content (from which the microbleed diameter was calculated) and average phase intensity; these boundaries were saved to prevent double counting. As a means to organize and easily reference CMBs, each slice was divided into four quadrants: upper left (1^{st} quadrant), upper right (2^{nd} quadrant), lower right (3^{rd} quadrant) and lower left (4^{th} quadrant). For each scan, CMBs were numbered sequentially from the dorsal side of the brain. If a particular slice contained more than one MB, numbers would be assigned within each quadrant.

In a process often marked by uncertainty, a helpful guideline can be used if CMBs are taken to be less than 6 mm in diameter (18,19): a CMB (by definition) may be seen in at most three adjacent 2-mm-thick slices before disappearing. A vessel would generally appear in more than three slices and/or would be identified as such in the mIP. Likewise, focal hypointensities seen at bifurcations of vessels can be discriminated with a similar analysis and use of the mIP.

Given our longitudinal data, a potential CMB's location, size and appearance over time factored into the general confidence of its identification. For example, given two potential CMBs of equal size and of similar behavior over time, the one located within the white matter—away from heavily vascularized areas—would be counted with more certainty than one in the cortical gray matter or along the sylvian fissure. Additionally, a CMB that is uncertain in one scan, but appears more clearly on later scans will be counted with greater confidence than one that cannot be checked longitudinally. In this regard, and after a blinded review of all scans, the first-year scans were used as baseline controls for CMB identification in subsequent scans.

RESULTS

Out of the 103 total cases, 97 were found to have had 0 to 3 CMBs in either their first or last scans. Here, we shall focus on the results of a secondary analysis of the remaining six cases, which had more than 3 CMBs in their first or last scans (see Table 1). Half of these six cases were scanned annually for three years, while the other half had annual scans for four years. One of these patients died after year 4.

After a period of four years, 16 out of the 75 MCI subjects converted to progressive cognitive impairment (PCI) based on CDR scores. Six out of these 16 had more than four

CMBs in their final scans as well as an increasing number of CMBs over time. An account of all CMBs observed over time in these six patients is given in Table 1 and a comparison of MCI patients with controls is shown in Table 2. Figure 3 shows a histogram of CMB diameters from the six patients' last scans. The remaining 10 PCI subjects had less than four CMBs seen on any one scan. (The 59 MCI subjects who failed to convert to PCI also had less than 4 CMBs on any one scan.) No significant association was found between the presence of WMH and baseline cognitive classification (normal vs. MCI) indicating a generalized distribution in both groups.

The six cases described in the present work were all part of the 41 MCI patients independently evaluated by three raters, with rater 1 differing from rater 3 by 33 counts out of 317, and rater 2 differing from rater 3 by 24 counts out of 317, amounting to inter-rater agreements of 89.6% and 92.4%, respectively. The interclass correlation for all three reviewers was 0.985. After consultation with a neuroradiologist experienced at interpreting SWI, four out of 134 total unique CMBs were removed to arrive at the final counts, amounting to a 97% agreement between evaluations by the three trained observers and the neuroradiologist.

Microbleed Characterization

Given the high resolution afforded by SWI, oftentimes we were able to detect subtle changes in a given CMB's size year-to-year (Fig. 4). CMBs were frequently observed to be increasing in size over time.

An observation seen in the six PCI cases of interest concerns the appearance of larger bleeds over time. Of these six cases, four were seen to have bleeds larger than 4 mm in diameter in their frontal, parietal or occipital lobes. Subject 3 in Table 1 had a major vascular abnormality in the right frontal lobe of the brain (Fig. 5). The first scan of this subject shows that there is no indication of abnormality in the first scan. However, on the second scan (taken five months later) there is evidence of subarachnoid hemosiderosis, most likely following a hemorrhage. In the last two scans, the hemosiderosis appears to further increase in size, with scans 2 and 3 showing a possible source of the blood draining into the parenchyma (see Fig. 5, arrows).

Subject 4 had two larger CMBs: one in the thalamus on the left side of the brain (Fig. 2c) and the other in the right side of the brain just above the cerebellum (Fig. 6). For the thalamic bleed, there was no change in size over time and it can be observed in all three scans. However, the other bleed does appear to get larger from the second scan to the third (taken 15 months later). Figure 7 shows a dramatic increase in CMBs in the right parietal lobe of subject 5, who converted to PCI between scans 2 and 3.

Volume measurements were done for each CMB found in the six patients' last scans and each CMB's diameter was calculated. A histogram of the diameters of all 130 CMBs measured appears as Figure 3. It has been shown that SWI not only detects more CMBs compared to conventional GRE T2*, but also enables the detection of CMBs smaller in size (20). Figure 3 supports these findings by demonstrating that most CMBs detected in this study were only 1–3 mm in diameter. Although Figure 3 represents bleeds counted in the patients' final scans, an interesting finding was that most newly developed CMBs were observed to be of a smaller diameter (data not shown here).

In this study, a total of 16 patients converted from mild to progressive cognitive impairment based on CDR scores. The six cases with MBs that we have discussed were all found to belong to the PCI group.

DISCUSSION

Given the high correlation between histologically detected CMBs and those detected on GRE T2* in previous studies (21,22), we are quite confident that the hypointensities seen on SWI represent CMB-related hemosiderin deposits. Due to a lack of confirmatory pathological data, it is difficult to distinguish between PCI that is related to progressive microvascular pathology (CAA, microinfarcts, microbleeds) and progressive development of microfibrillary tangles and amyloid plaques. Accordingly, perhaps the most appropriate categorization for the observed cognitive decline with increasing CMB is dementia with associated microvascular pathology. One interpretation of the role of these microbleeds is the work of Jellinger, who proposed that the role of the microvasculature in late-onset cognitive decline was synergistic with parenchymal plaques and tangles (11).

Among the recommendations for improved quality standards in the diagnosis of dementia set forth in 2001 by the American Academy of Neurology (23) is the critical need for biomarkers that have been evaluated by a longitudinal study. This study addresses this recommendation from one perspective. Our subjects' progression from MCI to PCI suggests that for a subset of patients having probable vascular disease, an MCI diagnosis along with a longitudinal increase in CMBs can be used to predict dementia onset. Specifically, our results show that all six MCI patients with four or more CMBs became progressively demented. In this regard, SWI-detected CMBs can be seen as a prospective marker for microvasculopathy.

SWI has three advantages over standard clinical GRE T2* that make it especially well-suited for CMB detection: 1) the use of phase information; 2) its high resolution; and 3) its long TE, which contributes to an increased susceptibility effect. A recent review by Greenberg, et al. (24) has set forth several guidelines for the radiologic detection of CMBs. While meeting the requirements intrinsic to the criteria of a 3D GRE T2* sequence, the current SWI study offers the added benefits of minimized CMB mimics such as calcification, vessel flow voids and the presence of deoxyhemoglobin. SWI filtered phase data is able to discriminate between calcium and hemosiderin because diamagnetic calcium carbonate appears with the opposite-sign phase as paramagnetic hemosiderin (25). Further, vessel flow voids can be discounted as a CMB confounder because SWI is flow compensated. Finally, venous deoxyhemoglobin is easily dismissed as a hemosiderin mimic by following our CMB scoring methods and using the mIP. The use of 2 mm-thick slices further contributes to increased MB sensitivity (14).

Recent data suggest that high resolution 3D GRE T2* is able to image significantly more CMBs than 2D (26). SWI's sensitivity to hemosiderin—a byproduct of microbleeding—has made it possible for us to detect microbleeds as small as 1 mm^3 (1 voxel) in size. Recent work by Greenberg, et al. (27) suggests a cut-off of 5.7 mm between diameters of microbleeds and marcobleeds when using a conventional GRE sequence. As can be seen in Figure 3, however, most CMBs counted with SWI in our study were less than 4 mm in diameter, as expected for a higher-sensitivity sequence. SWI is more sensitive to the detection of CMBs compared to conventional GRE and GRE-EPI because of its high resolution and its use of phase information (20). In fact, in studies of CMBs in trauma, SWI revealed six times more hemorrhages than conventional gradient-echo imaging (28).

The local fields produced by hemosiderin lead not only to T2* signal loss but also to changes in phase. In our study, we used SWI filtered phase images as a means to detect and map CMBs and to detect changes in iron content (as described by Haacke, et al. (29)). It is possible to have a situation where bleeding occurs so uniformly that there are negligible T2* effects, but a significant phase change makes the bleed visible in SWI when it would not

have been in a conventional magnitude gradient-echo image (30). Generally, as in conventional gradient-echo imaging, there will be a blooming effect or a loss in signal larger than the true size of the object. However, with high resolution SWI there is limited blooming and the phase information is high-pass filtered, keeping the information used to produce the SW images local (13,30).

We found that there was more error in locating CMBs when only a single time point was used to evaluate the images. However, with the longitudinal data available to us, these errors were dramatically reduced and in the six cases reported here all reviewers had to agree on a CMB before it was included in Table 1. This stepwise comparison along with the magnitude, phase and mIP data required many days of careful evaluation for each patient.

Calcifications can also cause signal loss, especially in the deep cerebral structures of the basal ganglia. However, we tended to not find CMBs here, perhaps because patients with hypertension were excluded from this study. Deep CMBs were found only in Patient 4 (Fig. 2, Table 1), which may suggest a contribution from atherosclerotic microangiopathy (6).

As can be seen from Figure 1, the prevalence of 1 or more CMBs did not differ much between MCI (14%) and healthy controls (11%). As reported in Roob, et al. (4), 1 to 5 CMBs have been seen per person in a cognitively normal, aged group. However, unlike the present work, Roob, et al.'s study contained all hypertensive patients, perhaps accounting for the large prevalence of CMBs observed in the basal ganglia of these patients. The similar rates of 14% and 11% are unsurprising considering the results of Jeerakathil, et al. (5), who reported a prevalence of 12.6% for their elderly cohort.

It is important to draw attention to the agreement of our observed increasing CMB counts over time with the steady worsening of our six subjects' cognitive functioning as measured by their clinical dementia ratings (Figure 10). Adding to this the fact that four out of these six subjects developed larger bleeds seems to make our findings relevant for the prediction of "probable vascular" dementia. The hallmarks for this diagnosis include a clearly documented temporal relationship between a bleed and the onset of dementia, clinical dementia characteristics, and evidence of at least one infarct outside the cerebellum (31). Although none of the four patients with larger bleeds had a history of infarction, their steadily degenerating neurological and clinical features strongly suggest a risk of additional hemorrhagic lesions and the development of probable ischemic vascular dementia. Further follow-up scans will need to be performed to monitor for cerebral infarcts and strokes.

A wealth of research is currently blurring the line between vascular dementia and AD, going so far as to suggest that sporadic AD be classified as a vascular disorder rather than as a neurodegenerative one (32). The small CMBs so well-detected by SWI could be causative in nature but this remains to be evaluated. We see the present study as a potential contributor to this ongoing discussion.

In conclusion, a four-year longitudinal study of patients progressing from MCI to PCI has made it possible for us to follow the development of cerebral microbleeds over time and to categorize them using SWI. It appears that if an MCI patient has five or more CMBs, the patient will progress to more serious dementia over time, possibly reflecting a putative loss in parenchymal function.

Acknowledgments

Grant Support

This work was supported in part by the National Institutes of Health Grant AG20948, the State of Michigan Grant 085P5200251 and Siemens Medical Solutions.

The authors would like to thank Darren Fuerst, PhD for his assistance with the statistics and Lisa Hamm for helping to edit the manuscript.

REFERENCES

1. Walker DA, Broderick DF, Kotsenas AL, Rubino FA. Routine use of gradient-echo MRI to screen for cerebral amyloid angiopathy in elderly patients. AJR Am J Roentgenol. 2004; 182(6):1547–1550. [PubMed: 15150006]
2. Imaizumi T, Horita Y, Hashimoto Y, Niwa J. Dotlike hemosiderin spots on T2*-weighted magnetic resonance imaging as a predictor of stroke recurrence: a prospective study. J Neurosurg. 2004; 101(6):915–920. [PubMed: 15597750]
3. Won Seo S, Hwa Lee B, Kim EJ, et al. Clinical significance of microbleeds in subcortical vascular dementia. Stroke. 2007; 38(6):1949–1951. [PubMed: 17510457]
4. Roob G, Schmidt R, Kapeller P, Lechner A, Hartung HP, Fazekas F. MRI evidence of past cerebral microbleeds in a healthy elderly population. Neurology. 1999; 52(5):991–994. [PubMed: 10102418]
5. Jeerakathil T, Wolf PA, Beiser A, et al. Cerebral microbleeds: prevalence and associations with cardiovascular risk factors in the Framingham Study. Stroke. 2004; 35(8):1831–1835. [PubMed: 15155954]
6. Vernooij MW, van der Lugt A, Ikram MA, et al. Prevalence and risk factors of cerebral microbleeds: the Rotterdam Scan Study. Neurology. 2008; 70(14):1208–1214. [PubMed: 18378884]
7. Kirsch W, McAuley G, Holshouser B, et al. Serial Susceptibility Weighted MRI Measures Brain Iron and Microbleeds in Dementia. J Alzheimers Dis. 2009
8. Vinters HV. Cerebral amyloid angiopathy. A critical review. Stroke. 1987; 18(2):311–324. [PubMed: 3551211]
9. Koennecke HC. Cerebral microbleeds on MRI: prevalence, associations, and potential clinical implications. Neurology. 2006; 66(2):165–171. [PubMed: 16434647]
10. Cordonnier C, Al-Shahi Salman R, Wardlaw J. Spontaneous brain microbleeds: systematic review, subgroup analyses and standards for study design and reporting. Brain. 2007; 130(Pt 8):1988–2003. [PubMed: 17322562]
11. Jellinger KA, Lauda F, Attems J. Sporadic cerebral amyloid angiopathy is not a frequent cause of spontaneous brain hemorrhage. Eur J Neurol. 2007; 14(8):923–928. [PubMed: 17662016]
12. Werring DJ. Cerebral microbleeds: clinical and pathophysiological significance. J Neuroimaging. 2007; 17(3):193–203. [PubMed: 17608904]
13. Haacke EM, Xu Y, Cheng YC, Reichenbach JR. Susceptibility weighted imaging (SWI). Magn Reson Med. 2004; 52(3):612–618. [PubMed: 15334582]
14. Nandigam RN, Viswanathan A, Delgado P, et al. MR imaging detection of cerebral microbleeds: effect of susceptibility-weighted imaging, section thickness, and field strength. AJNR Am J Neuroradiol. 2009; 30(2):338–343. [PubMed: 19001544]
15. Petersen RC, Smith GE, Waring SC, Ivnik RJ, Tangalos EG, Kokmen E. Mild cognitive impairment: clinical characterization and outcome. Arch Neurol. 1999; 56(3):303–308. [PubMed: 10190820]
16. Wahlund LO, Barkhof F, Fazekas F, et al. A new rating scale for age-related white matter changes applicable to MRI and CT. Stroke. 2001; 32(6):1318–1322. [PubMed: 11387493]
17. Artero S, Tiemeier H, Prins ND, Sabatier R, Breteler MM, Ritchie K. Neuroanatomical localisation and clinical correlates of white matter lesions in the elderly. J Neurol Neurosurg Psychiatry. 2004; 75(9):1304–1308. [PubMed: 15314121]
18. Imaizumi T, Honma T, Horita Y, et al. Dynamics of dot-like hemosiderin spots on T2*-weighted MRIs associated with stroke recurrence. J Neuroimaging. 2007; 17(3):204–210. [PubMed: 17608905]
19. Greenberg SM, Eng JA, Ning M, Smith EE, Rosand J. Hemorrhage burden predicts recurrent intracerebral hemorrhage after lobar hemorrhage. Stroke. 2004; 35(6):1415–1420. [PubMed: 15073385]

20. Akter M, Hirai T, Hiai Y, et al. Detection of hemorrhagic hypointense foci in the brain on susceptibility-weighted imaging clinical and phantom studies. Acad Radiol. 2007; 14(9):1011–1019. [PubMed: 17707307]
21. Fazekas F, Kleinert R, Roob G, et al. Histopathologic analysis of foci of signal loss on gradient-echo T2*-weighted MR images in patients with spontaneous intracerebral hemorrhage: evidence of microangiopathy-related microbleeds. AJNR Am J Neuroradiol. 1999; 20(4):637–642. [PubMed: 10319975]
22. Tatsumi S, Shinohara M, Yamamoto T. Direct comparison of histology of microbleeds with postmortem MR images: a case report. Cerebrovasc Dis. 2008; 26(2):142–146. [PubMed: 18560217]
23. Knopman DS, DeKosky ST, Cummings JL, et al. Practice parameter: diagnosis of dementia (an evidence-based review). Report of the Quality Standards Subcommittee of the American Academy of Neurology. Neurology. 2001; 56(9):1143–1153. [PubMed: 11342678]
24. Greenberg SM, Vernooij MW, Cordonnier C, et al. Cerebral microbleeds: a guide to detection and interpretation. Lancet Neurol. 2009; 8(2):165–174. [PubMed: 19161908]
25. Wu Z, Mittal S, Kish K, Yu Y, Hu J, Haacke EM. Identification of calcification with MRI using susceptibility-weighted imaging: a case study. J Magn Reson Imaging. 2009; 29(1):177–182. [PubMed: 19097156]
26. Vernooij MW, Ikram MA, Wielopolski PA, Krestin GP, Breteler MM, van der Lugt A. Cerebral microbleeds: accelerated 3D T2*-weighted GRE MR imaging versus conventional 2D T2*-weighted GRE MR imaging for detection. Radiology. 2008; 248(1):272–277. [PubMed: 18490493]
27. Greenberg SM, Nandigam RN, Delgado P, et al. Microbleeds versus macrobleeds: evidence for distinct entities. Stroke. 2009; 40(7):2382–2386. [PubMed: 19443797]
28. Tong KA, Ashwal S, Obenaus A, Nickerson JP, Kido D, Haacke EM. Susceptibility-weighted MR imaging: a review of clinical applications in children. AJNR Am J Neuroradiol. 2008; 29(1):9–17. [PubMed: 17925363]
29. Haacke EM, Ayaz M, Khan A, et al. Establishing a baseline phase behavior in magnetic resonance imaging to determine normal vs. abnormal iron content in the brain. J Magn Reson Imaging. 2007; 26(2):256–264. [PubMed: 17654738]
30. Xu Y, Haacke EM. The role of voxel aspect ratio in determining apparent vascular phase behavior in susceptibility weighted imaging. Magn Reson Imaging. 2006; 24(2):155–160. [PubMed: 16455403]
31. Chui HC, Victoroff JI, Margolin D, Jagust W, Shankle R, Katzman R. Criteria for the diagnosis of ischemic vascular dementia proposed by the State of California Alzheimer's Disease Diagnostic and Treatment Centers. Neurology. 1992; 42(3 Pt 1):473–480. [PubMed: 1549205]
32. de la Torre JC. Alzheimer disease as a vascular disorder: nosological evidence. Stroke. 2002; 33(4):1152–1162. [PubMed: 11935076]

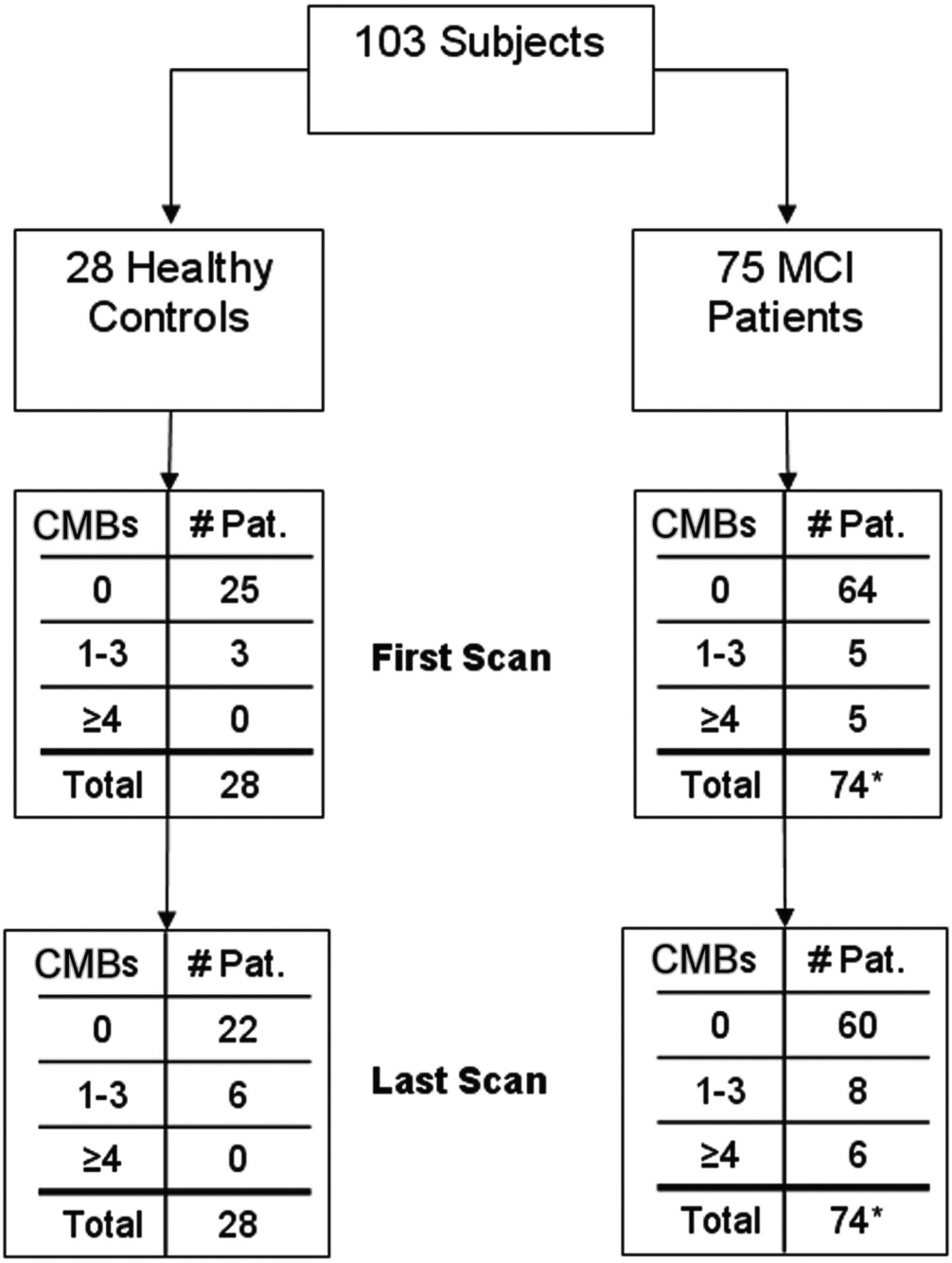

Figure 1.
Breakdown of subjects.
*One patient was not evaluated due to poor image quality.

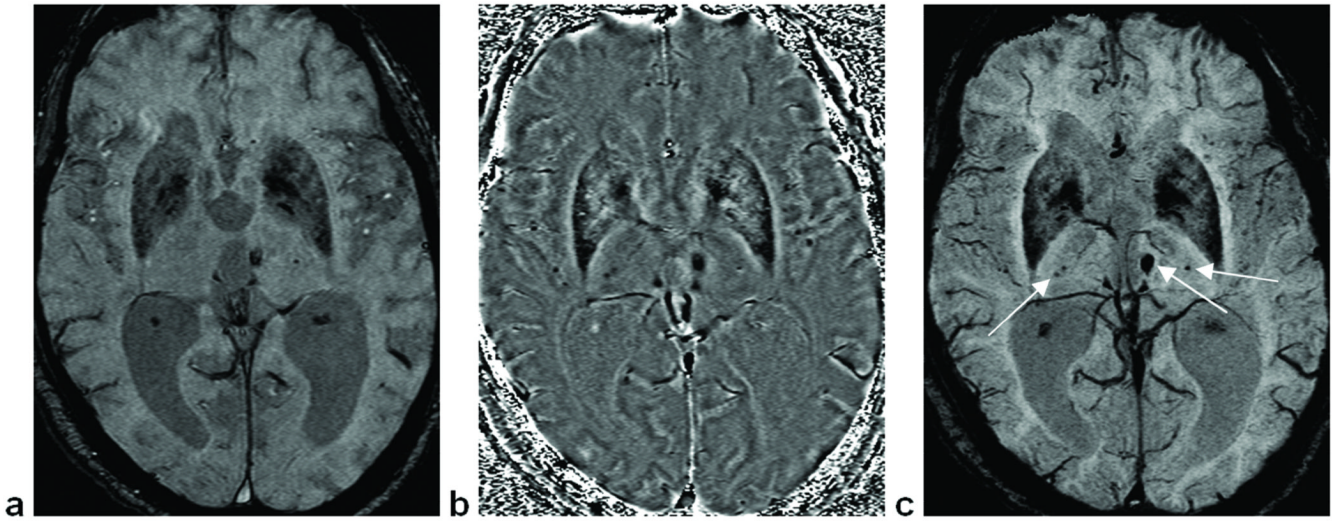

Figure 2.

Images used for the evaluation of microbleed counts. **(a)** Original magnitude image. **(b)** SWI high pass filtered phase image, which gives additional information compared to the original magnitude image. **(c)** SWI mIP over five slices (a product of combining magnitude and phase information), showing 4 deep CMBs.

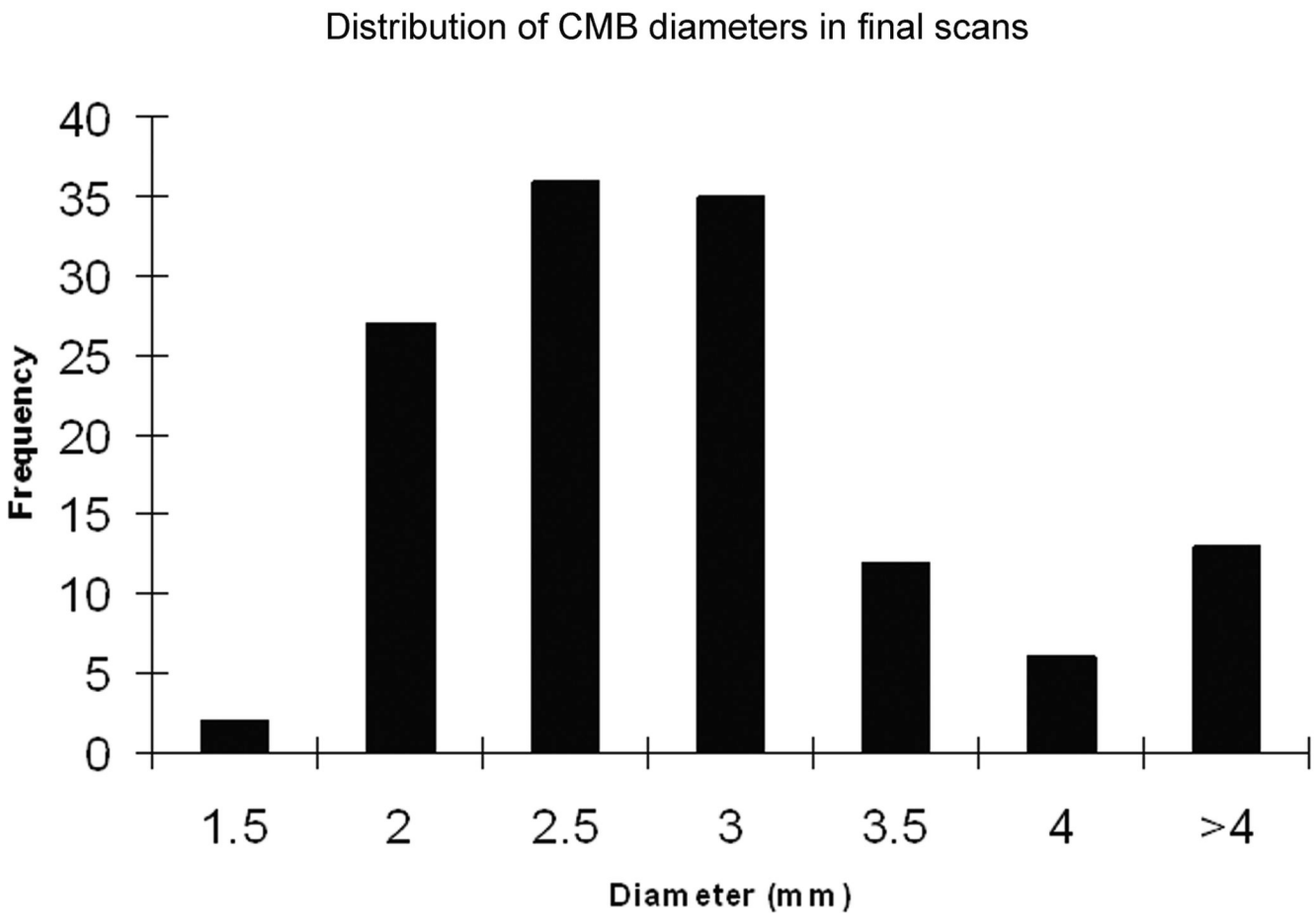

Figure 3.
Histogram showing a Rayleigh-like distribution for CMBs ≤ 4 mm in diameter.

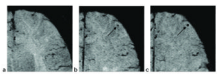

Figure 4.
An example of a CMB increasing in size over time. **(a)** No evidence of a CMB in the first scan. **(b)** In the second scan, a CMB appears in the left frontal lobe. **(c)** In the third scan, the CMB has increased in size. Images are SWI mIPs over 5 slices.

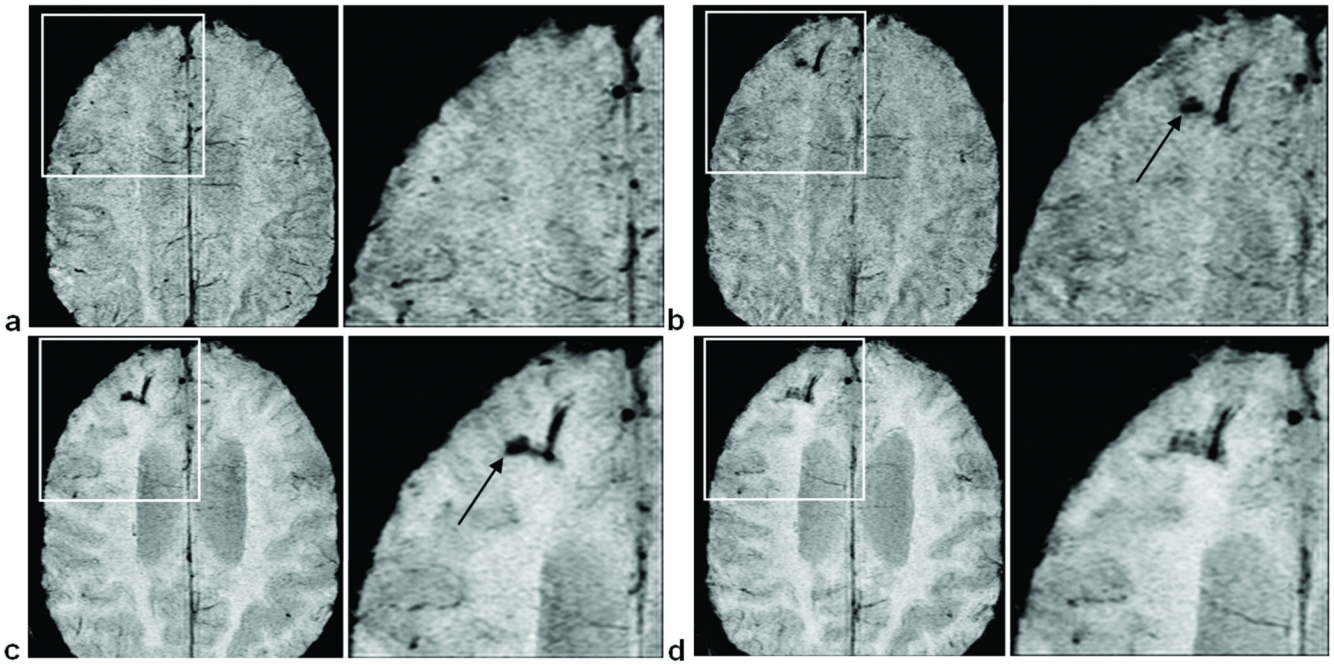

Figure 5.

Right-frontal subarachnoid hemosiderosis in the gray matter spreading into the parenchyma over time. Images **(a)** through **(d)** are from successive scans, each approximately one year apart. Arrows in scans **(b)** and **(c)** depict a possible source of the bleed. Images are mIPs over 5 slices.

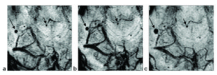

Figure 6.

(a)–(c) Images of subject 4 showing a relatively large CMB increasing in size over three scans (long arrow). The short arrow shows a CMB of constant size, indicating that the bleed's larger appearance cannot be blamed on distortion or artifact. Images are mIPs over 5 slices.

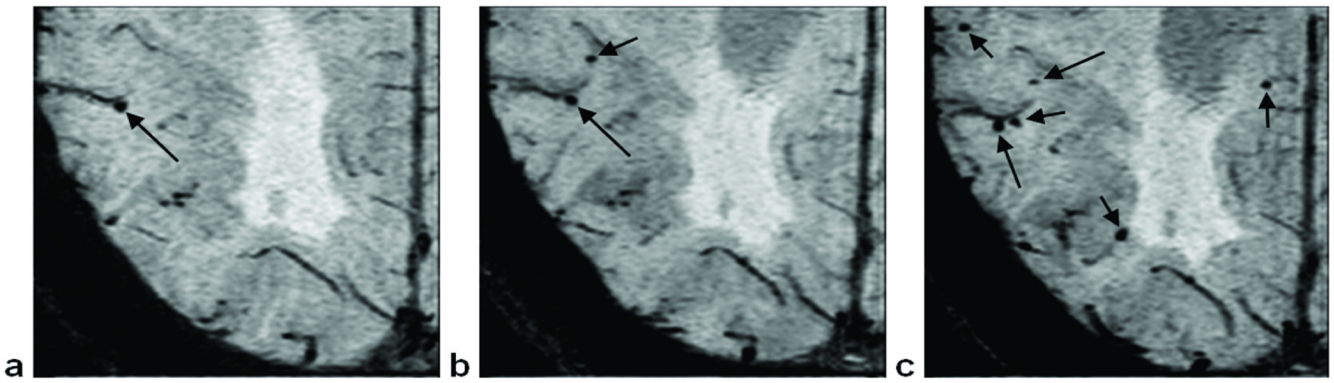

Figure 7.

Three time points for the same subject showing the stepwise development of CMBs in the right parietal lobe. The first scan **(a)** contains one CMB (arrow). The second scan **(b)**, taken one year later, reveals a new CMB (short arrow). After another nine months, scan 3 **(c)** shows four more CMBs (short arrows). Images are mIPs over 5 slices.

Table 1

Numbers of CMBs (lobar/deep) observed in each scan for each subject having over 3 CMBs in any one scan.

Subject No.	Scan 1	Scan 2	Scan	Scan 4
1	8/0	16/0	28/0	**40/0**
2	5/0	**6/0**	**6/0**	**6/0**
3	2/0	2/0	**4/0**	**5/0**
4*	28/7	29/7	33/8	-
5	6/0	9/0	**9/0**	-
6	12/0	**16/0**	**37/0**	-

Fourth scans not available for subjects 4–6. Counts in bold are at dementia status.

* This patient was deemed a PCI case after scan 3.

Table 2

Comparison of CMB counts between the first and last scans of MCI patients and controls.

Number of CMBs	Number of MCI Subjects		Number of Controls	
	1st Scan	Last Scan	1st Scan	Last Scan
0	64	60	25	22
1 – 3	5	8	3	6
>3	5	6	0	0
Total	74*	74*	28	28

*One data set from the MCI group was not analyzed because of poor image quality.